Exogenous carbon monoxide protects against mitochondrial DNA-induced hippocampal pyroptosis in a model of hemorrhagic shock and resuscitation

LAN FU[1,2], DONG-XUE ZHANG[3], LI-MIN ZHANG[4], YAN-CHENG SONG[2], FENG-HAI LIU[2], YAN LI[4], XU-PENG WANG[4], WEI-CHAO ZHENG[4], XIAO-DONG WANG[4], CHUN-XIAO GUI[4], XIANG-JUN KONG[5] and LI-QING KANG[2]

[1]Graduate School, Tianjin Medical University, Tianjin 300070; Departments of [2]Radiodiagnosis, [3]Gerontology and [4]Anesthesiology; [5]Central Laboratory, Cangzhou Central Hospital, Cangzhou, Hebei 061001, P.R. China

Received September 29, 2019; Accepted January 29, 2020

DOI: 10.3892/ijmm.2020.4493

Abstract. Carbon monoxide-releasing molecule-3 (CORM-3), which is an exogenous carbon monoxide (CO) compound, slowly releases CO under physiological conditions; this exerts neuroprotective effects against incomplete ischemia/reperfusion injury. The objective of the present study was to investigate whether the administration of CORM-3 protects against nucleotide-binding oligomerization domain-like receptor pyrin domain-3 (NLRP3) inflammasome formation and neuronal pyroptosis in the hippocampus following hemorrhagic shock and resuscitation (HSR). To establish this, an HSR model was created. Hemorrhagic shock was induced in adult male Sprague-Dawley rats under sevoflurane anesthesia by bleeding using a heparinized syringe to maintain a mean arterial pressure of 30±5 mmHg for 60 min. Resuscitation was performed by reperfusion of the blood and, if necessary, administering sterile saline to achieve the baseline arterial pressure. Following resuscitation, CORM-3 (4 mg/kg) was injected via the femoral vein. Neuronal pyroptosis in the hippocampus, mitochondrial morphology, mitochondrial DNA (mtDNA), brain magnetic resonance imaging, expression levels of NLRP3 and the interaction of pro-caspase-1 and apoptosis-associated speck-like protein containing a CARD domain (ASC) were examined 12 h after HSR; locomotor activity was assessed 7 days after HSR. Compared with HSR-treated rats, CORM-3 administration resulted in a lower level of neuronal pyroptosis in the hippocampus, improved mitochondrial morphology, a lower mtDNA level, steadier levels of metabolites, decreased expression levels of NLRP3 and pro-caspase-1 interacting with ASC and enhanced locomotor activity. In conclusion, treatment with CORM-3 ameliorated impairments of locomotor and exploratory activities in a rat model of HSR. The mechanism may be associated with the inhibition of mitochondrial DNA-induced pyroptosis via improvements in cell metabolism.

Correspondence to: Dr Li-Qing Kang, Department of Radiodiagnosis, Cangzhou Central Hospital, 16 Xinhua West Road, Cangzhou, Hebei 061001, P.R. China
E-mail: kangliqing2019@126.com

Abbreviations: CORM, carbon monoxide-releasing molecule; HSR, hemorrhage shock and resuscitation; NLRP3, nucleotide-binding oligomerization domain-like receptors pyrin domain-3; MRS, magnetic resonance spectroscopy

Key words: carbon monoxide, neuroprotection, pyroptosis, mitochondrial DNA, NLRP3

Introduction

Long-term hypoxia induced by hemorrhagic shock, cross-clamping of major vascular structures and extracorporeal circulation may lead to incomplete ischemic brain injury during the perioperative period (1-3). Inflammatory cytokines, such as interleukin-1β (IL-1β) and IL-18, have previously been implicated in neuronal cell death and functional injuries following incomplete cerebral ischemia/reperfusion (4). The inactive precursors of IL-1β are activated into mature inflammatory cytokines by cleaved caspase-1, which mediates a type of programmed cell death termed pyroptosis (5). Pyroptosis contributes to the development of ischemia/reperfusion-related diseases, such as stoke and acute kidney injury (6,7). As key strategies for incomplete ischemia/reperfusion therapy, relieving secondary neuronal pyroptosis and improving surviving neuronal function are currently in development (8).

Carbon monoxide (CO), which is a type of neurotoxic molecule, has valuable cytoprotective effects, including positive and negative alterations of heme-containing enzymatic function and modulation of numerous cellular targets, such as extracellular signal-regulated kinase 1/2 (9). Exogenously administered CO affects cell metabolism and supports oxidative phosphorylation and mitochondrial respiration, enhancing ATP production and cellular energy status (10). Carbon monoxide-releasing molecule (CORM)-3 has emerged as an excellent alternative to CO administration (11) and has been demonstrated to provide protection in inflammation and ischemia/reperfusion injury models by inhibiting the activation of nucleotide-binding oligomerization domain-like receptors pyrin domain-3 (NLRP3) inflammasome, which contains

NLRP3, apoptosis-associated speck-like protein containing a CARD domain (ASC) and pro-caspase-1, in sepsis and metabolic diseases (12,13). IL-1β and IL-18 maturation and release are controlled by activated NLRP3 inflammasomes (14).

Whether CORM-3 reduces locomotor activity degeneration in a model of blood loss and re-infusion remains unclear. The present study aimed to examine whether CO derived from CORM-3 served a protective role against mitochondrial DNA-induced neuronal pyroptosis following hemorrhagic shock and resuscitation (HSR) by inhibiting cellular metabolism and NLRP3 inflammasome activation.

Materials and methods

Animals. The National Institutes of Health Guidelines for the Care and Use of Laboratory Animals were followed while performing all animal experiments in this study. The Animal Review Board of Cangzhou Central Hospital provided formal approval to conduct the experiments. Male Sprague-Dawley rats (Charles River Laboratories, Inc.) aged between 9 and 10 weeks (weight, 350-400 g) were housed in individual shoebox cages with bedding. The room temperature was maintained at 25±1˚C with a 12-h alternating light/dark cycle. The health and behavior of rats were monitored every day. The rats were euthanized by exsanguination from the abdominal aorta under sevoflurane anesthesia (3-4%) at time points indicated below. Electrocardiographic monitoring was used to verify death.

HSR protocol. An HSR model was developed as previously described (15,16). Rats were allowed free access to water and chow until the start of the experiments. Sevoflurane (7-8% for induction and 3-4% for maintenance) was used for anesthetizing tracheally-intubated rats with a volume-controlled ventilator (tidal volume, 4 ml/100 g; initial respiratory frequency, 70 bpm; FiO_2, 40%; ALC-V; Shanghai Alcott Biological Technology Inc.). A handheld end-tidal carbon dioxide/oxygen saturation monitor (PMSH-300; SunLife Science, Inc.) was used to adjust the respiratory frequency to an end-tidal carbon dioxide pressure of 35-40 mmHg. The rats underwent cannulation with a heparinized indwelling needle (22 G) via the left femoral artery for blood pressure measurements and via the left femoral vein to induce hemorrhage shock. To maintain a mean arterial pressure of 30±5 mmHg for 60 min, hemorrhagic shock was induced by bleeding into a heparinized syringe (10 U/ml). Resuscitation was performed by reperfusion of all shed blood and, if necessary, administration of sterile saline to reach the baseline arterial pressure as described in our previous studies (15,16). Next, 4 mg/kg CORM-3 was injected intravenously (cat. no. S744801; Selleck Chemicals). Catheters to the left femoral artery and vein were inserted using an indwelling needle (22 G) as a surgical preparation in the Sham group; the vehicle control was an equivalent volume of normal saline injection. Inactive CORM-3 (iCORM-3) was prepared by dissolving CORM-3 in PBS and incubating it for 24 h under air and light exposure at 25˚C; to remove residual CO, the solution was bubbled with 100% nitrogen.

Measurement of IL-1β and IL-18 levels. At 3, 6, 12 and 24 h after resuscitation, rats were euthanized (n=6 per group) and total protein was extracted from the hippocampal tissues by RIPA Lysis Buffer (cat. no. P0013D; Beyotime Institute of Biotechnology). ELISA kits (Interleukin-1β Assay kit, cat. no. H002; Interleukin-18 Assay kit, cat. no. H015; Nanjing Jiancheng Bioengineering Institute) were used to measure IL-1β and IL-18 levels according to the manufacturer's protocol.

Immunofluorescence. At 12 h after resuscitation, rats (n=6 per group) were anesthetized with sevoflurane and perfused with 10% neutral-buffered formalin to fix the cerebral tissues. The tissues were embedded in paraffin, cut into 5-μm sections and underwent immunofluorescence staining to determine the degree of neuronal pyroptosis. Briefly, the paraffin sections were dewaxed and hydrated (100% ethanol for 3 min, 95% ethanol for 2 min, 80% ethanol for 2 min, 75% ethanol for 2 min, H_2O for 1 min) for 10 min at room temperature, followed by incubation with primary polyclonal rabbit anti-cleaved caspase-1 (1:200; cat. no. ab1872; Abcam) and polyclonal mouse anti-neuronal nuclei (NeuN; 1:500; cat. no. ab104224; Abcam) antibodies or NeuN antibody alone overnight at 4˚C. The sections were washed three times in PBS and incubated in the dark for 1 h at 25˚C in a blocking solution containing the secondary antibodies (Cy^3-conjugated goat anti-rabbit IgG; cat. no. A0516; or FITC-conjugated goat anti-mouse IgG; cat. no. A5608; both from Beyotime Institute of Biotechnology) diluted 1:200 in the blocking solution. Subsequently, 5 μg/ml DAPI (Beyotime Institute of Biotechnology) was added for 2 min to identify the cell nuclei. Propidium iodide (PI; Beyotime Institute of Biotechnology) was added for 2 min to identify dead cells. A laser scanning confocal microscope (Olympus Corporation) was used to capture immunofluorescence images; A total of six fields at x200 magnification were randomly selected from three sections in each group. The mean densitometry of the fluorescence signal in each field was analyzed by Image-pro plus 6.0 software (Media Cybernetics, Inc.). The percentage of cleaved caspase-1 or PI combined with NeuN- and DAPI-positive cells was calculated.

Measurement of lactate dehydrogenase (LDH). At 12 h after resuscitation, homogenates were prepared using hippocampal tissues (n=6 per group) as described above; following centrifugation at 1,000 x g and 4˚C for 10 min, the supernatant was used to detect the content of lactic dehydrogenase (LDH) using an LDH Cytotoxicity Assay kit (cat. no. C0016, Beyotime Institute of Biotechnology) by spectrophotometry at 492 nm (BioTek Epoch).

MRI study. A clinical 3.0 T MRI scanner (DISCOVERY MR 750; GE Healthcare) was used to perform MRI with a special coil in rats at room temperature. The following parameters were used to acquire coronal fast spin echo T2-weighted images: Repetition time (TR)/echo time (TE), 3500/85; number of excitations (NEX), 2; phase, 256; frequency, 320; slices, 21; slice thickness, 1.5 mm; field of view, 80 mm; and acquisition time, 2 min. At 3, 6, 12, and 24 h after HSR, the rats (n=6 per group) were anesthetized with sodium pentobarbital (65 mg/kg) and placed prone in an animal holder, and the coil was positioned and fixed over the head of the animal. T2W images displaying the CA1 region of the hippocampus were analyzed. The regions of interest were placed free-hand on the hippocampus and the signal intensity (SI) was measured in addition to visual inspection. T2-weighted standardized signal intensity (SSI)

was obtained by calculating the ratios between the average SI and the temporalis SI to reflect the signal changes on T2WI. As a measure of the T2W images for each rat, the SSI ratios before/after indicated stimuli were determined.

^{1}H-magnetic resonance spectroscopy (MRS) spectra were acquired using multivoxel pattern analysis in the right hemisphere of the rat brain covering the hippocampus. The following parameters were used to acquire the ^{1}H-MRS images: TR/TE, 1500/35; NEX, 1; phase, 18; frequency, 16; and acquisition time, 7 min 18 sec. The GE Function Tool software (AW 4.5 Workstation; GE Healthcare) was used to perform spectral image analysis and data processing to analyze the spectrum signal with MR. For background modeling, the metabolite area under the peak was quantified using a quantum estimation method with a subtraction approach. To estimate peak areas, a simulated basis set was used. A relative quantification method using the Cr peak as the internal spectral reference was applied to reduce systematic variations between animals. The N-acetylaspartate (NAA)/creatinine (Cr), myoinositol (mI)/Cr, and lipid (Lip)/Cr ratios were statistically evaluated. Each MRS metabolite was identified by the part per million (ppm) position of the nuclear spectrum, including NAA (2.02 ppm), Cr (3.05 ppm), mI (2.2 ppm) and Lip (0.9 ppm).

Open field test. On day 7 after HSR, open field test was used to assess locomotor and exploratory activities (n=12 per group). To track the movement of the rats, the open field apparatus comprised a square opaque acrylic container (60x60 cm) and a video camera fixed 1 m above the arena. Prior to testing, the rats were allowed to acclimatize to the room for 1 h; the open field boxes were disinfected to remove any smells that could affect behavior. The tests were performed in the breeding room. Each rat was placed in the middle of the chamber for each trial. After 1 min of adaptation, the behavior of the rat was recorded for 5 min prior to returning to their home cages in the same room during the interval between trials, and the open field box was cleaned with a damp cloth. To analyze the images, a computerized tracking system (XR-XZ301; Shanghai Xinruan Software Co., Ltd.) was used. The distance, speed, rearing events, time in all corners and grooming event number were analyzed. After the test, all rats were euthanized by exsanguination from the abdominal aorta under sevoflurane anesthesia.

Mitochondria extraction and electron microscopy. The mitochondria from the hippocampal tissues were extracted 12 h after HSR (n=6 per group) (17). Briefly, the hippocampal tissue homogenates were centrifuged twice at 1,000 x g and 4˚C for 5 min, and the supernatant was centrifuged at 15,000 x g and 4˚C for 2 min. After carefully eliminating all fat and fluffy layers on the top of the pellet containing the mitochondria, the supernatant was removed. The pellets from the two tubes were combined, resuspended in 1.5 ml ice-cold PBS and centrifuged at 15,000 x g and 4˚C for 2 min to eliminate harmful enzymes, nucleases, phospholipases and proteases. The final pellet was resuspended in ice-cold final equilibrated buffer (250 mM sucrose, 5 mM KH_2PO_4, 10 mM Tris-HCl, 2 mg/ml BSA, pH 7.2) and fixed in 2.5% glutaraldehyde in 0.1 M sucrose phosphate buffer (SPB) for 1 h at room temperature. Following washing with 0.1 M SPB, the mitochondrial extractions were fixed with 1% osmium tetroxide in 0.1 M SPB for 1 h at room temperature and the pellets were dehydrated with ethanol at 10, 30, 70 and 99% for 30 min, infiltrated with LR white resin (Sigma-Aldrich; Merck KGaA), embedded in capsule beams and polymerized at 65˚C for 48 h. Serial ultrathin slices (50 nm) were cut with an ultramicrotome and stained with 4% uranyl acetate-lead citrate for 3 min at room temperature, and transmission electron microscopy (JEM-2000EX; JEOL, Ltd.) was used to observe the ultrastructure of the mitochondrial pellets. The dysmorphic mitochondria were examined and counted at x3,000 magnification, including swelling and ghost or normal mitochondria, as described previously (18). Dysmorphic mitochondria were characterized by the following parameters: i) Degenerative changes, such as matrix vacuolation, disarrangement of cristae, swelling and partial cristolysis; and ii) necrosis, characterized by complete cristolysis or ghost cells as described in our previous study (15).

Measurement of ATP content. Isolated mitochondria (n=6 animals per group) were used to measure ATP synthesis with a luciferase/luciferin-based system as previously described (19). The ATP Assay kit (cat. no. S0027; Beyotime Institute of Biotechnology) was used to measure ATP content according to the manufacturer's protocol.

Mitochondrial DNA quantification. At 12 h after resuscitation, the rats (n=6 per group) were sacrificed as described above. DNA from the hippocampal tissues was harvested using the Wizard SV Genomic DNA Purification System (Promega Corporation) according to manufacturer's instructions. mtDNA levels were measured by normalizing the mitochondrial cytochrome b gene (MT-CYB; gene ID, Rn03296746_s1) to the nuclear heat shock protein 70 (Hspa1a; gene ID, Rn00583013_s1) gene. All samples were replicated three times in a 25-ml reaction volume containing 50 ng sample DNA and 2X Probe RT-Mastermix (Qiagen, Inc.) with both probes in each well. The MT-CYB probe was labeled with hexachloro fluorescein, and the Hspa1a probe was labeled with carboxy-fluorescein. The following amplification conditions were used: 95˚C for 15.05 min, followed by 45 cycles of 95˚C for 15 sec and 60˚C for 1 min. The $2^{-\Delta\Delta Cq}$ method was used to quantify the gene expression levels.

Western blotting. At 12 h after HSR, total protein was extracted from the hippocampal tissues (n=6 per group) as described in the IL-1β and IL-18 assay. Samples containing 30 μg protein quantified by bicinchoninic acid (BCA) assay were separated by 10% SDS-PAGE and transferred onto a PVDF membrane. The membrane was blocked with 5% skimmed milk at 37˚C for 2 h, and primary antibodies rabbit anti-rat polyclonal cleaved caspase-1 (1:1,000; cat. no. ab1872; Abcam), monoclonal NLRP3 (1:1,000; cat. no. ab210491; Abcam), polyclonal Gasdermin D (GSDMD; 1:1,000; cat. no. ab219800; Abcam), polyclonal IL-1b (1:1,000; cat. no. K107559P; Beijing Solarbio Science & Technology Co., Ltd.) and polyclonal IL-18 (1:1,000; cat. no. K002143P; Beijing Solarbio Science & Technology Co., Ltd.) were applied at 4˚C overnight, followed by incubation with a horseradish peroxidase-conjugated goat anti-rabbit IgG secondary antibody (1:2,000; cat. no. sc-2004; Santa Cruz Biotechnology, Inc.) at 25˚C for 1 h. Protein bands in each treatment group were detected using an enhanced chemiluminescence western blot detection system ImageJ 1.48u

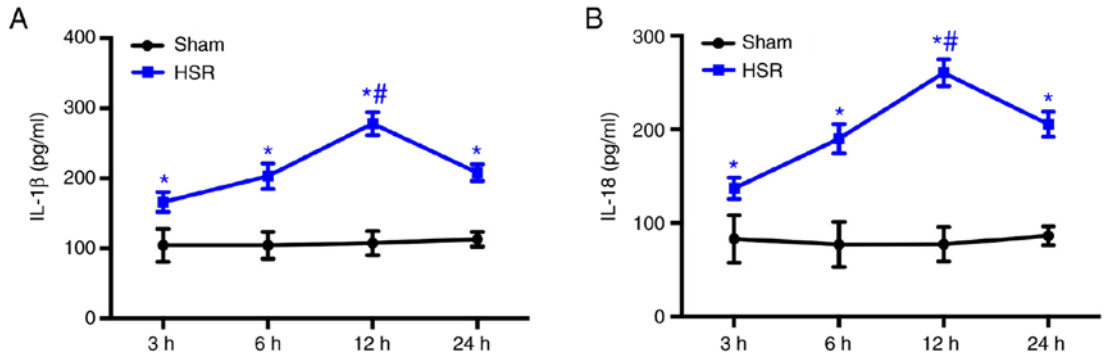

Figure 1. CORM-3 via femoral vein injection after resuscitation ameliorates upregulation in the expression of (A) IL-1β and (B) IL-18 in the hippocampal tissue. Data are presented as the mean ± SD (n=6 per group). *P<0.05 vs. Sham; #P<0.05 vs. other time points of the HSR group. CORM, carbon monoxide-releasing molecule; HSR, hemorrhage shock and resuscitation; IL, interleukin.

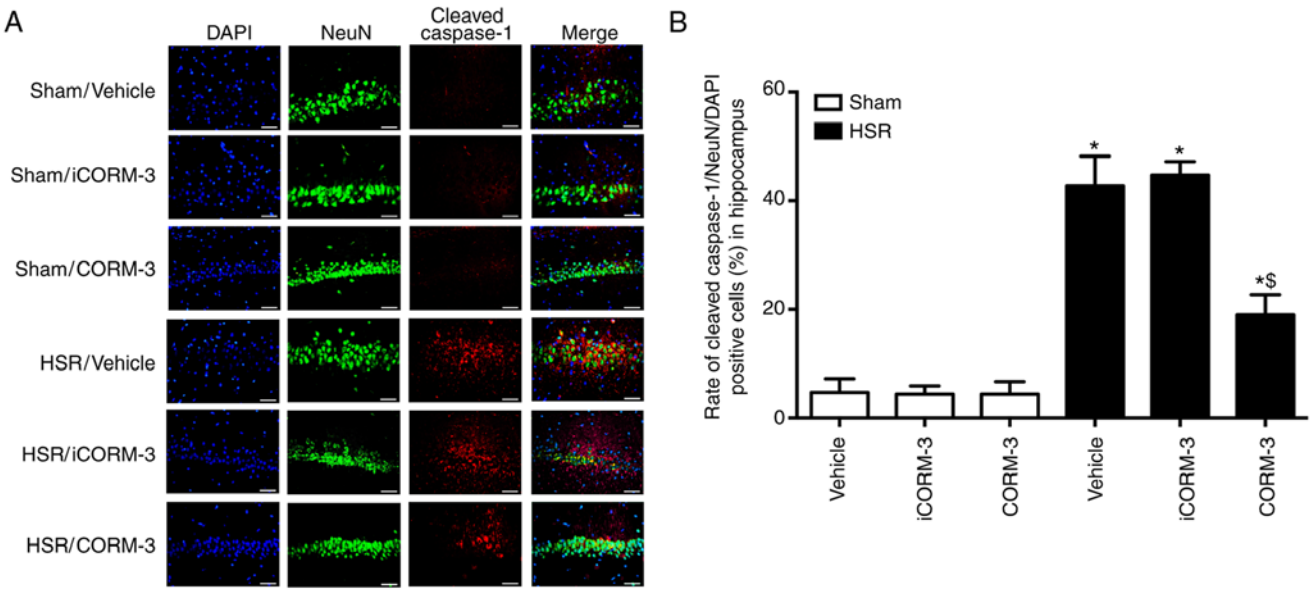

Figure 2. CORM-3 ameliorates upregulation in pyroptosis in the hippocampus. (A) Representative photomicrographs of cleaved caspase-1/NeuN/DAPI staining (cleaved caspase-1, red; NeuN, green; DAPI, blue) demonstrating pyroptotic cells in the hippocampal tissue induced by the indicated stimuli. Scale bar, 50 μm. (B) Percentages of pyroptotic cells in the hippocampal tissue induced by the indicated stimuli. Data are presented as the mean ± SD (n=6 per group). *P<0.05 vs. Sham; $P<0.05 vs. HSR vehicle and HSR iCORM-3. CORM, carbon monoxide-releasing molecule; HSR, hemorrhage shock and resuscitation; iCORM-3, inactive CORM-3.

software (National Institutes of Health). β-actin (1:2,000; cat. no. sc-47778; Santa Cruz Biotechnology, Inc.) was used as an internal reference (20).

Co-immunoprecipitation (Co-IP). Total protein was extracted from the hippocampal tissues (n=6 per group) 12 h after HSR and lysed in tissue lysis buffer as described above. Following centrifugation at 15,000 x g and 4˚C for 10 min, the supernatant was collected, and the protein concentration was measured with a BCA protein assay. Rabbit anti-ASC polyclonal antibodies (3 μg) were added to 500 μg tissue lysate and incubated at 4˚C for 60 min with gentle mixing. After incubation with 20 μl Protein A/G Plus-Agarose beads (Santa Cruz Biotechnology, Inc.) overnight at 4˚C, the resultant mixture was centrifuged at 4,000 x g and 4˚C for 5 min. The sample buffer was washed with PBS three times and added to the agarose beads. The samples were analyzed by western blotting as described above with antibodies against mouse ASC (1:500; cat. no. ab175449; Abcam), NLRP3 (1:500; cat. no. ab214185; Abcam) and β-actin (1:2,000; cat. no. sc-47778; Santa Cruz Biotechnology, Inc.).

Statistical analysis. SPSS 17.0 for Windows (SPSS, Inc.) was used to conduct all statistical analyses. Data are presented as the mean ± standard deviation. The Levene test was used to assess the assumption of homogeneity of variance. When data heteroscedasticity was identified, it was corrected by logarithmic transformation. A one-way analysis of variance followed by post hoc Bonferroni test was used to analyze the differences among groups. P<0.05 was considered to indicate a statistically significant difference.

Results

HSR induces increases in IL-1β and IL-18 levels. Rats were treated with hemorrhage shock for 1 h and resuscitated by blood perfusion to observe the effects of CORM-3 on HSR exposure. A total of 14 rats died after HSR, and the cause of

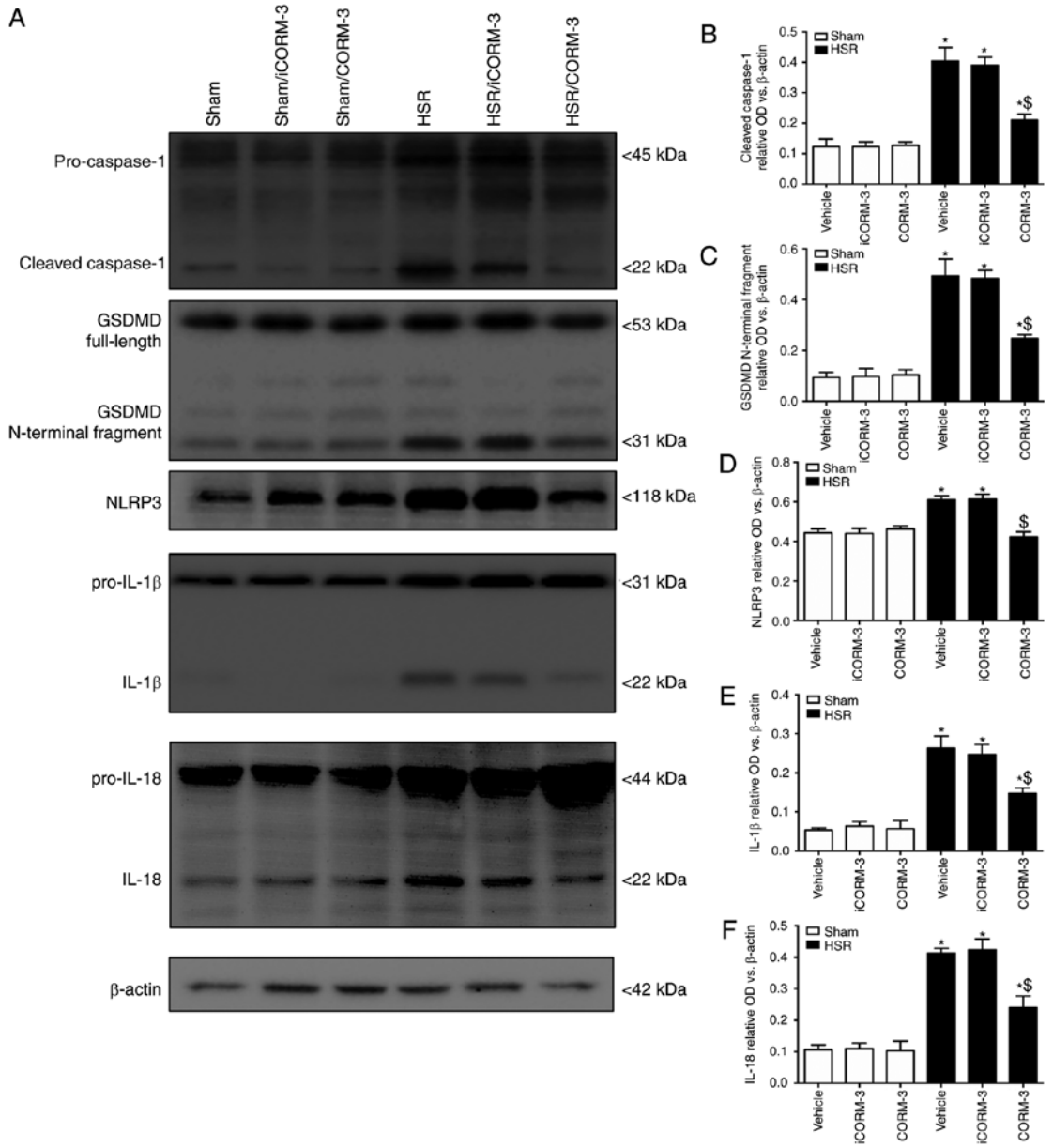

Figure 3. CORM-3 ameliorates upregulation in pyroptosis-associated protein expression in the hippocampus. (A) Representative western blots of cleaved caspase-1, GSDMD, NLRP3, IL-1β and IL-18 in the hippocampal tissue. (B-F) Relative expression levels of cleaved caspase-1, GSDMD, NLRP3, IL-1β and IL-18 in the hippocampal tissue evaluated by western blotting. Data are presented as the mean ± SD (n=6 per group). *P<0.05 vs. Sham; $P<0.05 vs. HSR vehicle and HSR iCORM-3. CORM, carbon monoxide-releasing molecule; HSR, hemorrhage shock and resuscitation; iCORM-3, inactive CORM-3; NLRP3, nucleotide-binding oligomerization domain-like receptors pyrin domain-3; IL, interleukin; GSDMD, Gasdermin D.

death determined by postmortem examination was mainly acute respiratory distress syndrome or pulmonary embolism. The IL-1β and IL-18 levels in the hippocampal tissue at different time points were assessed by ELISA assays. The results demonstrated that HSR significantly increased the levels of IL-1β and IL-18 at 3, 6, 12 and 24 h post-resuscitation compared with the sham group (P<0.05; Fig. 1A and B). Maximum IL-1β and IL-18 levels were observed at 12 h post-HSR (Fig. 1A and B).

CORM-3 protected against neuronal pyroptosis in the hippocampus after HSR. Immunofluorescence of cleaved caspase-1 combined with NeuN and DAPI was used to determine the effects of CORM-3 on neuronal pyroptosis at 12 h post-HSR (Figs. 2A and 3A). In the sham groups, a small number of hippocampal neurons exhibited the pyroptotic phenotype in the CA1 region of the hippocampus (positive for cleaved caspase-1 and NeuN; Fig. 2A and B). The number of cells of this type was notably increased in HSR-treated rats compared with the sham group (P<0.05; Fig. 2A and B). CORM-3-treated rats exhibited a reduced number of pyroptotic neurons double-stained with cleaved caspase-1 and NeuN compared with the vehicle and iCORM-3 groups (P<0.05), whereas the iCORM-3-treated group did not exhibit a reduction (Fig. 2A and B). Pyroptosis was also evaluated by determining the expression levels of cleaved caspase-1 (22 kDa), GSDMD (31 kDa), NLRP3, IL-1β, and IL-18 using western blotting; the results demonstrated that rats treated with CORM-3 after HSR exhibited lower expression levels of hippocampal cleaved caspase-1, GSDMD and NLRP3 compared with the HSR

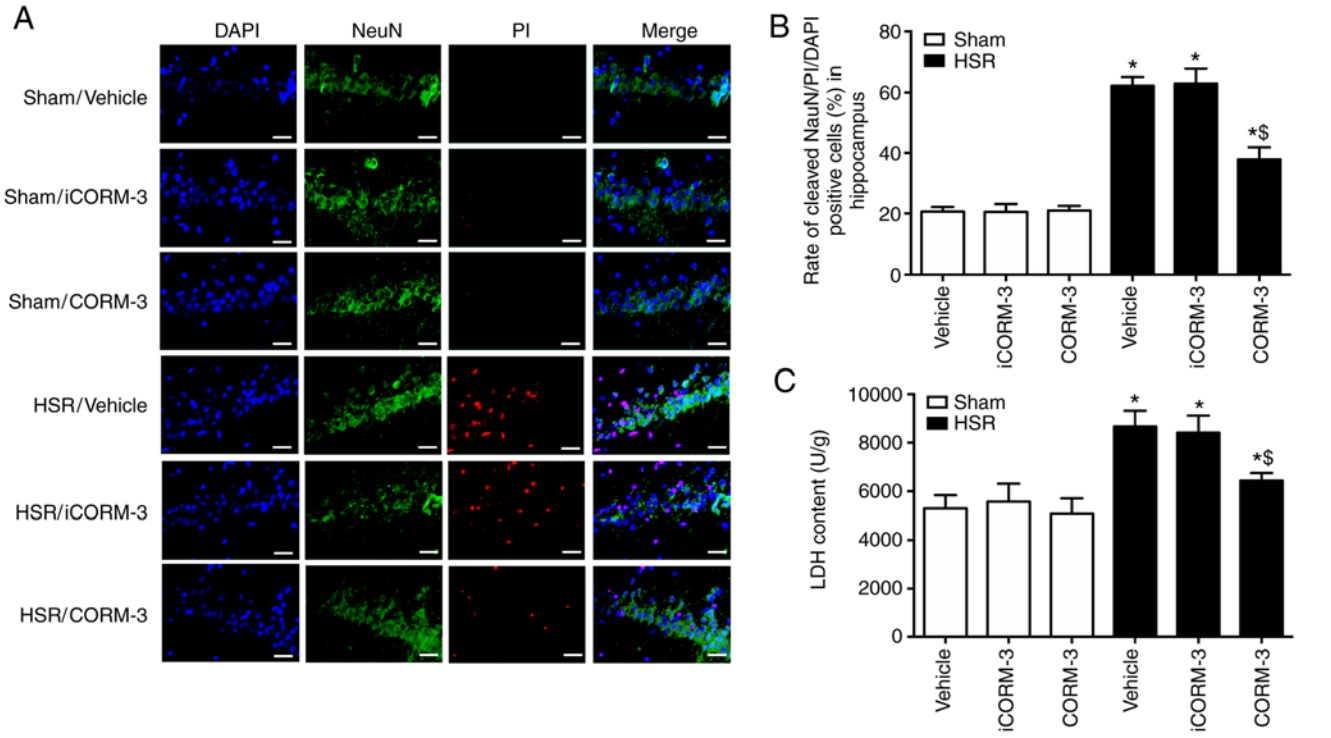

Figure 4. CORM-3 ameliorates HSR-induced neuronal death in the hippocampus. (A) Representative photomicrographs of NeuN/PI/DAPI staining (NeuN, green; PI, red; DAPI, blue) demonstrating neuronal death in the hippocampal tissue induced by the indicated stimuli. Scale bar, 50 μm. (B) Percentages of neuronal death in the hippocampal tissue induced by the indicated stimuli. (C) LDH content in the hippocampal tissue induced by the indicated stimuli. Data are presented as the mean ± SD (n=6 per group). *P<0.05 vs. Sham; $P<0.05 vs. HSR vehicle and HSR iCORM-3. CORM, carbon monoxide-releasing molecule; HSR, hemorrhage shock and resuscitation; iCORM-3, inactive CORM-3; PI, propidium iodide; LDH, lactate dehydrogenase.

iCORM-3- and vehicle-treated rats (P<0.05; Fig. 3A-D). As presented in Fig. 3E-F, similar results were observed for IL-1β and IL-18 expression levels.

NeuN-FITC/PI/DAPI staining was used for detecting neuronal death. The results revealed that CORM-3 notably decreased the number of NeuN-FITC/PI double-positive cells after HSR (P<0.05; Fig. 4A and B). A similar effect was observed using the LDH release assay, as LDH release was lower in HSR-treated rats after CORM-3 treatment compared with the HSR vehicle and iCORM-3 groups (Fig. 4C). In addition, the results also revealed that HSR significantly increased the ratio of SSI compared with the sham group (P<0.05; Fig. 5A and B). A similar effect was observed using the T2-weighted MRI assay, as demonstrated by the reduced SSI in HSR-treated rats after CORM-3 treatment compared with the iCORM-3 group (P<0.05; Fig. 5B). No significant differences were observed between the HSR vehicle and HSR iCORM-3 groups.

CORM-3 improves behavioral deficits in HSR-treated rats. To investigate the improvement in behavioral deficits induced by CORM-3 after HSR, locomotor and exploratory activities were assessed using an open field test 7 days post-resuscitation. Locomotion was indicated by total moving distance and average speed, whereas exploratory activity was represented by the scores of rearing/leaning and anxiety level reflected by time spent in the corner and the number of grooming events. Compared with the sham group, the HSR-treated rats exhibited a reduced traveling distance, slower moving speed, lower rearing/leaning scores, spent less time in the corner and grooming (P<0.05; Fig. 6). Although iCORM-3 treatment had no effects on these parameters, all values were improved in the HSR CORM-3 group compared with the HSR iCORM-3 group (P<0.05; Fig. 6). No significant differences were observed among the sham, sham iCORM-3 and sham CORM-3 groups.

MRS analysis of metabolites in the hippocampus of rats exposed to HSR. ^{1}H MRS was used to detect the metabolite ratios at 3, 6, 12 and 24 h post-HSR, revealing that significant changes in the hippocampus were notable at 3 h post-HSR for the NAA/Cr, mI/Cr and Lip/Cr ratios. The mI/Cr and Lip/Cr ratios increased, whereas NAA/Cr decreased within 24 h in the HSR iCORM-3 group compared with the Sham group (P<0.05; Fig. 7). HSR treatment induced the maximum NAA/Cr ratio at 12 h post-HSR (P<0.05; Fig. 7). CORM-3 administration partially reversed the changes in the NAA/Cr, mI/Cr and Lip/Cr ratios 3-24 h post-HSR compared with the HSR iCORM-3 group (P<0.05; Fig. 7).

CORM-3 improves mitochondrial dysfunction in HSR-treated rats. To investigate the improvements in mitochondrial dysfunction induced by CORM-3 after HSR exposure, the prevalence of dysmorphic mitochondria (Fig. 8A and B) and swelling and ghost mitochondria (Fig. 8A and C) were used to determine the mitochondrial morphology in the hippocampal tissue. A significant increase in the prevalence of dysmorphic mitochondria and swelling and ghost mitochondria, as well as a significant decrease in the level of ATP synthesis, were observed in the HSR iCORM-3 group compared with the sham group (Fig. 8B-D). CORM-3 treatment after HSR notably

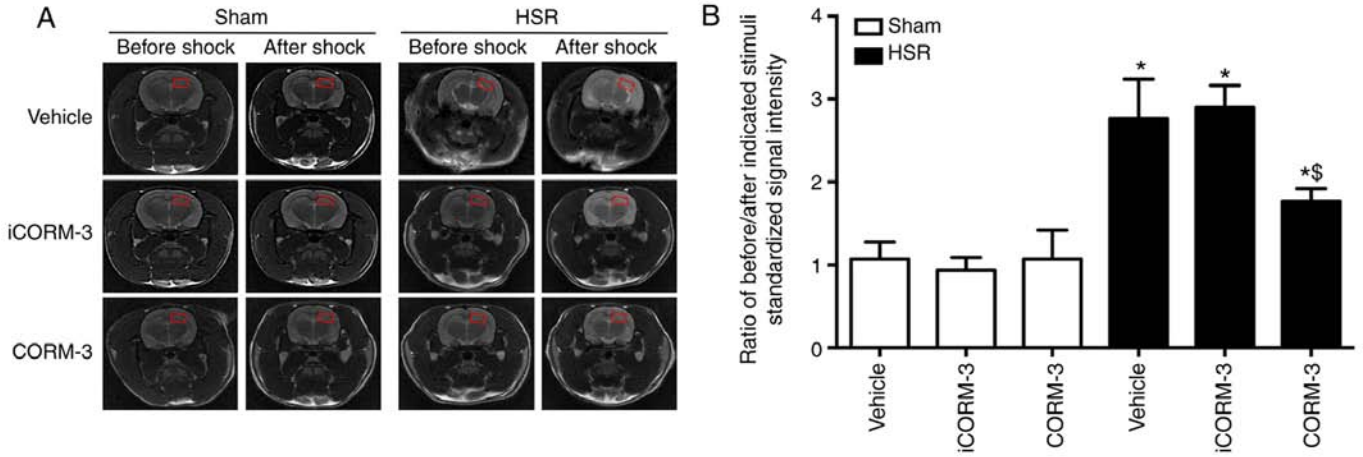

Figure 5. CORM-3 ameliorates the hyperintensity in T2-weighted MRI. (A) T2-weighted MRI coronal views from rats at 12 h after HSR. (B) The ratio of standardized signal intensity on regions of the cerebral hippocampus before/after hemorrhagic shock. Data are presented as the mean ± SD (n=6 per group). *P<0.05 vs. Sham; $P<0.05 vs. HSR vehicle and HSR iCORM-3. CORM, carbon monoxide-releasing molecule; HSR, hemorrhage shock and resuscitation; iCORM-3, inactive CORM-3.

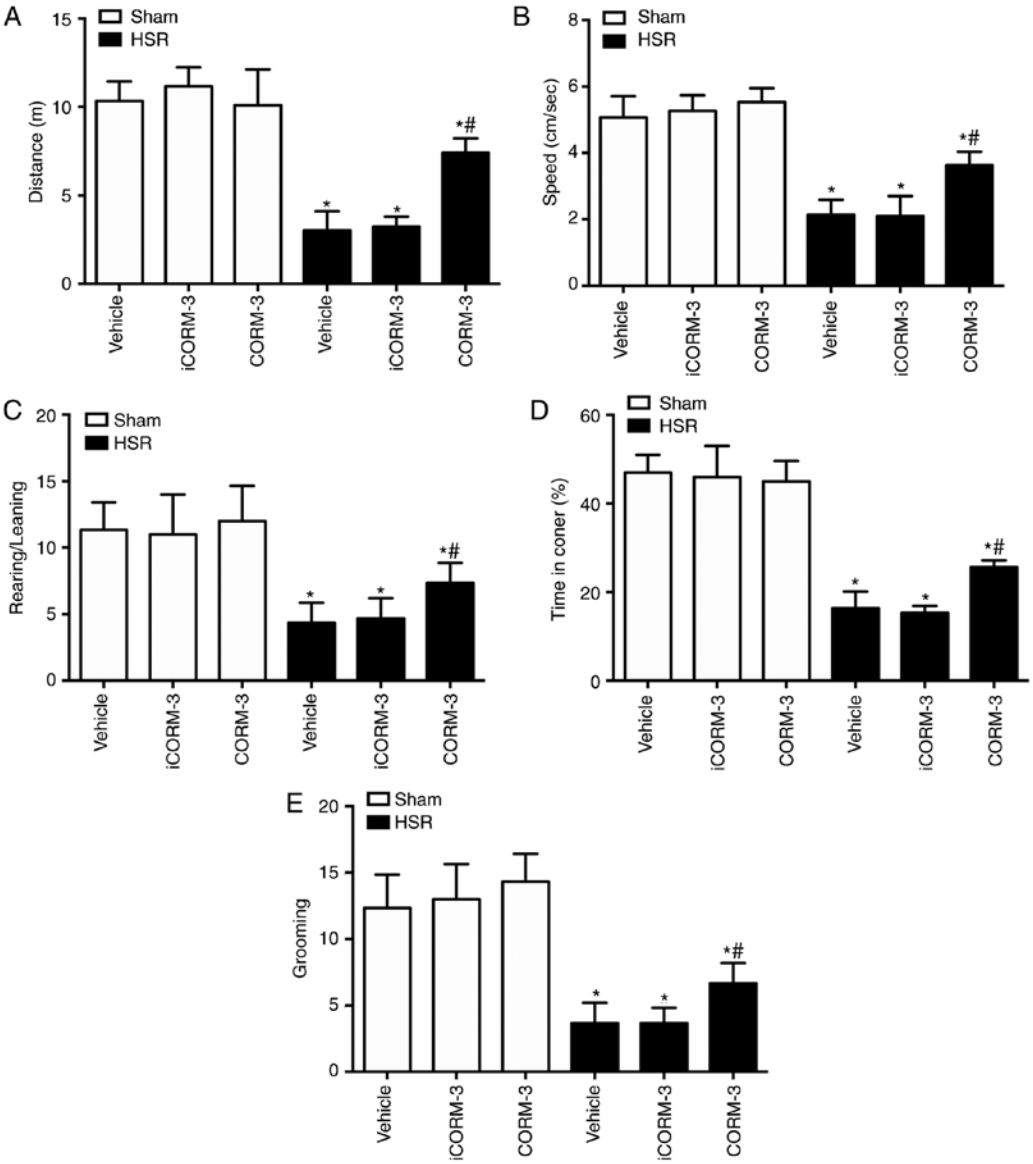

Figure 6. CORM-3 ameliorates impairments in locomotor and exploratory activities after HSR. (A) Distance, (B) speed, (C) rearing, (D) time in corner and (E) grooming of each group on day 7 after HSR. Data are presented as the mean ± SD (n=12 per group). *P<0.05 vs. Sham; #P<0.05 vs. HSR vehicle and HSR iCORM-3. CORM, carbon monoxide-releasing molecule; HSR, hemorrhage shock and resuscitation; iCORM-3, inactive CORM-3.

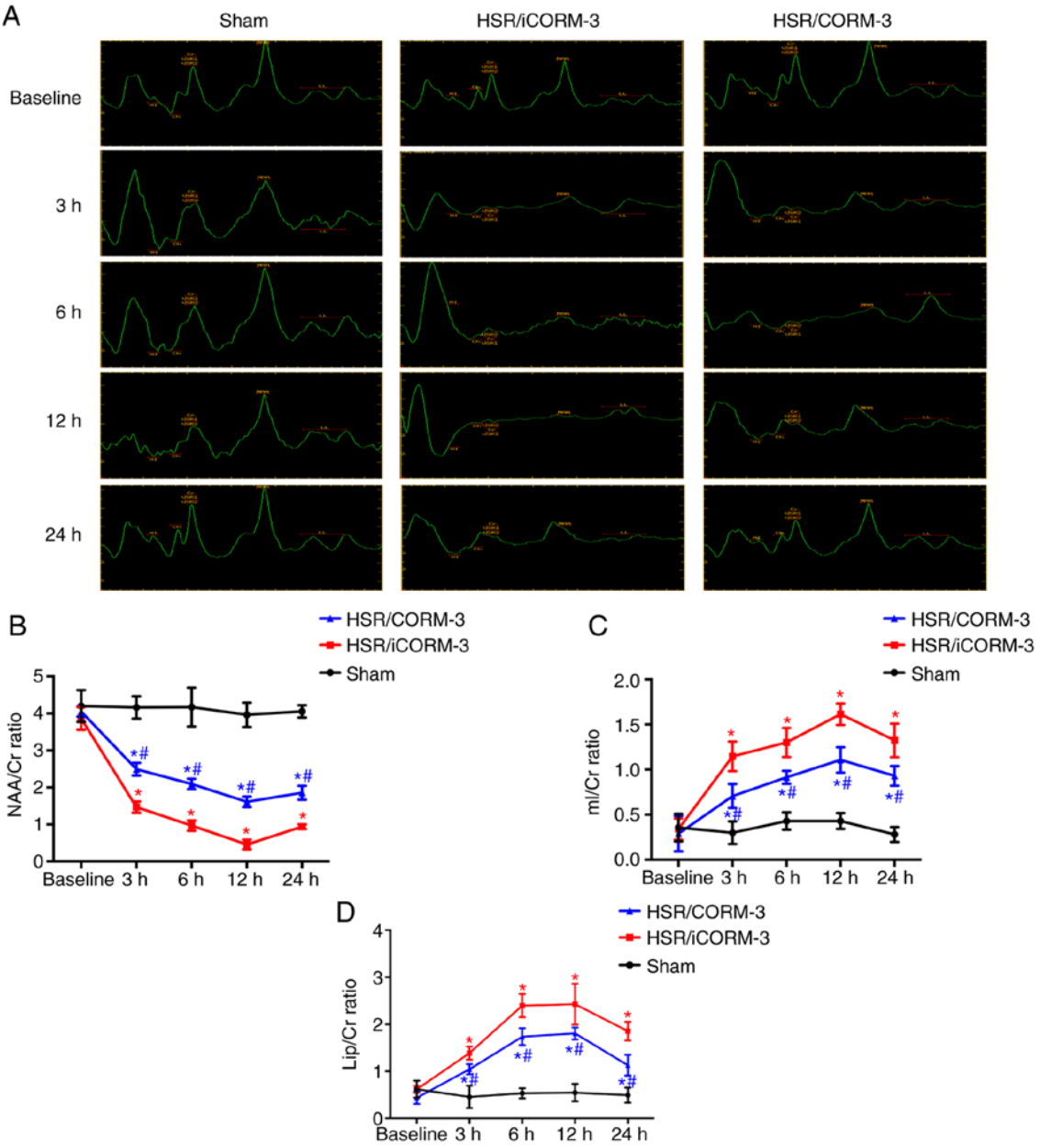

Figure 7. Time course of *in vivo* localized ^{1}H MR spectra in the hippocampus induced by the indicated stimuli. (A) Representative ^{1}H MR spectra of the hippocampus in the coronal view at 3, 6, 12 and 24 h after HSR treatment. (B-D) The time course of NAA/Cr, mI/Cr, and Lip/Cr ratios caused by the indicated stimuli. Data are presented as mean ± SD (n=6 per group). *P<0.05 vs. Sham; $^{\#}$P<0.05 vs. HSR iCORM-3. CORM, carbon monoxide-releasing molecule; HSR, hemorrhage shock and resuscitation; iCORM-3, inactive CORM-3; NAA, N-acetylaspartate; mI, myoinositol; Lip, lipid; Cr, creatinine.

improved mitochondrial morphology and ATP synthesis compared with the HSR iCORM-3 group. As presented in Fig. 8E, a similar result was also observed for total mtDNA in the cytosol, which was measured using the mitochondrial cytochrome b gene. CORM-3 administration after HSR significantly reduced the level of mtDNA compared with the HSR iCORM-3 group (P<0.05; Fig. 8E).

CORM-3 attenuates the interaction of pro-caspase-1/NLRP3/ASC after HSR. To determine how CORM-3 inhibits pro-caspase-1/NLRP3/ASC inflammasome activation, Co-IP was used to evaluate NLRP3-ASC and pro-caspase-1-ASC interactions. NLRP3 and ASC interactions were elevated in the HSR iCORM-3 group compared with the sham group, whereas CORM-3 partially inhibited these interactions (Fig. 9A). Similar results were observed for the pro-caspase-1-ASC interactions (Fig. 9B).

Discussion

The present study determined the effect of CORM-3 on HSR-induced neuronal dysfunction and provided evidence that exogenous CO derived from CORM-3 improved rat locomotor and exploratory activities after HSR. CORM-3 attenuated neuronal pyroptosis in the hippocampus and prevented subsequent NLRP3 inflammasome activation. In addition, CORM-3 improved mitochondrial morphology and metabolite ratios and decreased mtDNA levels in the cytosol.

The cause of death determined by postmortem examination was mainly acute respiratory distress syndrome or

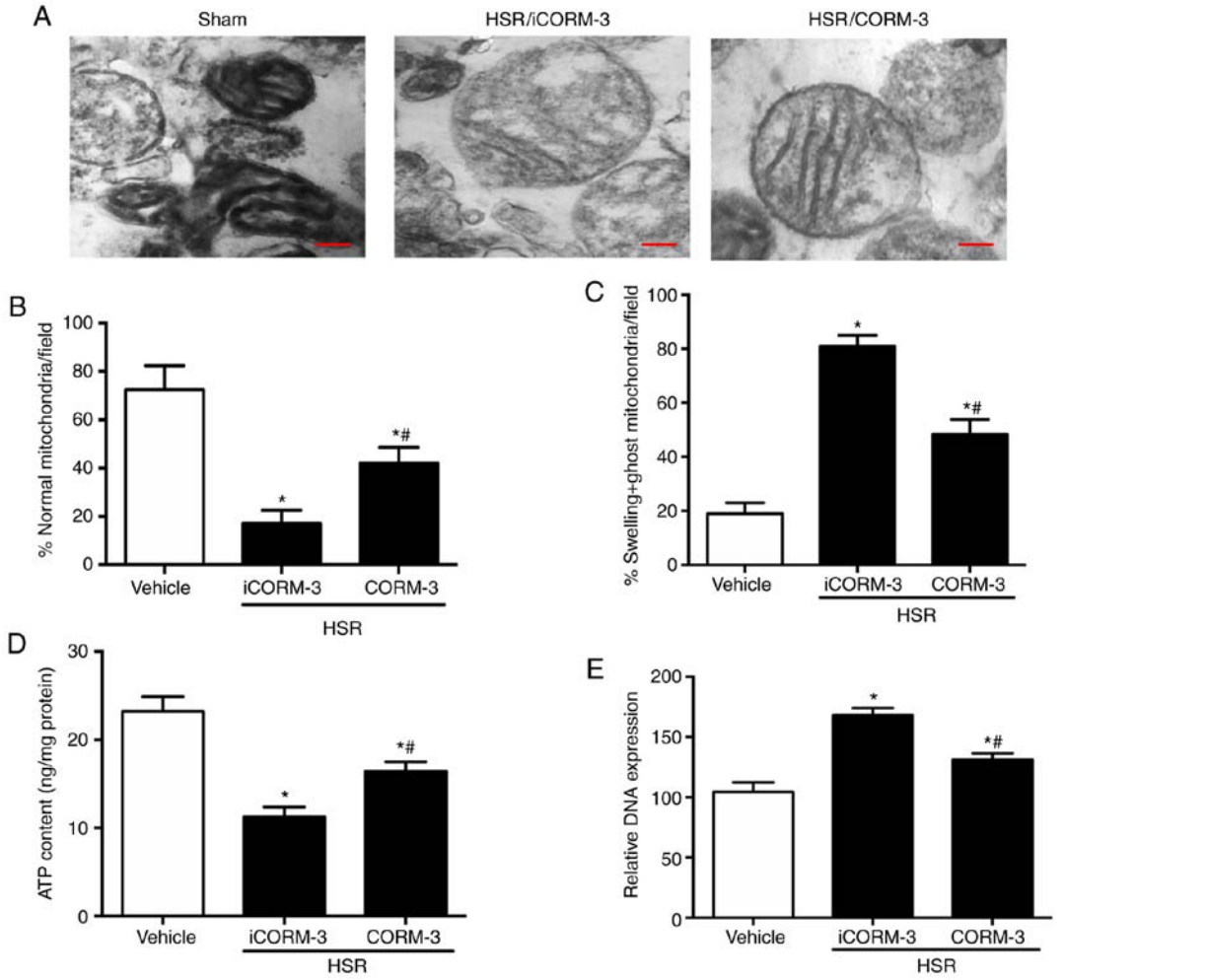

Figure 8. CORM-3 ameliorates mitochondrial dysfunction after HSR. (A) Dysmorphic hippocampal mitochondria induced by the indicated stimuli under an electron microscope. Scale bar, 200 nm. (B) Percentages of normal mitochondria in the hippocampal tissue induced by the indicated stimuli. (C) Percentages of swelling and ghost mitochondria in the hippocampal tissue induced by the indicated stimuli. (D) Changes in the mitochondrial ATP level induced by the indicated stimuli. (E) Changes in the mitochondrial DNA (mtDNA) induced by the indicated stimuli. Data are presented as the mean ± SD (n=6 per group). *P<0.05 vs. Sham; #P<0.05 vs. HSR iCORM-3. CORM, carbon monoxide-releasing molecule; HSR, hemorrhage shock and resuscitation; iCORM-3, inactive CORM-3.

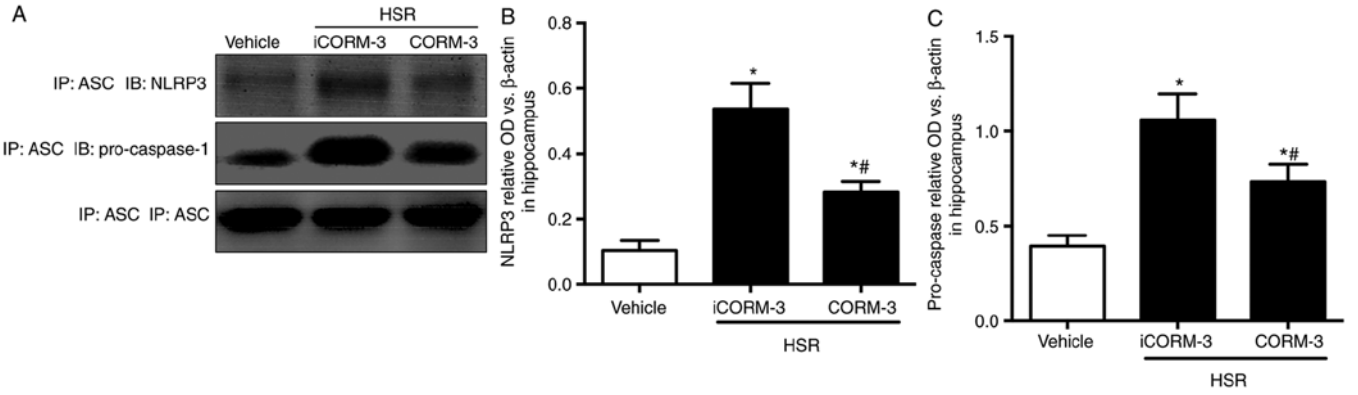

Figure 9. CORM-3 inhibits the interaction between NLRP3 and ASC in the hippocampus after HSR. (A) Co-immunoprecipitation assay with an anti-ASC antibody; hippocampal tissue was immunoblotted with anti-NLRP3, anti-pro-caspase-1 and anti-ASC antibodies. (B and C) Optical density values of (B) NLRP3 and (C) pro-caspase-1 in the hippocampal tissue evaluated by western blotting. Data are presented as the mean ± SD (n=6 per group). *P<0.05 vs. Sham; #P<0.05 vs. HSR iCORM-3. CORM, carbon monoxide-releasing molecule; HSR, hemorrhage shock and resuscitation; iCORM-3, inactive CORM-3; NLRP3, nucleotide-binding oligomerization domain-like receptors pyrin domain-3; ASC, apoptosis-associated speck-like protein containing a CARD domain.

pulmonary embolism, which was consistent with previous studies (21,22). Compared with previous study, the decreased mortality (8%) in this study may be associated with improved anesthesia and no trauma of laparotomy (22). Incomplete cerebral ischemia/reperfusion in a rat model of HSR induced severe neuronal apoptosis and pyroptosis in the hippocampus.

Pyroptosis, characterized as an inflammatory response, occurred in the early stage after reperfusion (within 24 h post-ischemia), but apoptosis occurred in the late stage after reperfusion (72 h to 7 days post-ischemia) in previous studies (15,16). In addition, a high level of neuronal pyroptosis in the cortical tissue is an important factor of HSR-induced decrease in learning and memory abilities (15). In the present study, the obtained results revealed that HSR caused neuronal pyroptosis in the hippocampus and impaired locomotor and exploratory activities, revealing that HSR-induced neurological dysfunction may be associated with neuronal pyroptosis in the hippocampus and may be characterized by caspase-1 activation and inflammatory factor release.

CORM-3 alleviated motor functional injury following spinal cord injury by inhibiting neuronal pyroptosis (23). In addition, CORM-3 attenuated the degeneration of learning and memory abilities following HSR mediated by inhibiting neuronal pyroptosis in the cortex (24). NLRP3 inflammasome activation is a multistep process that includes assembly of ASC and pro-caspase-1 (25). mtDNA from injured mitochondria has been reported to be fused in response to NLRP3 inflammasome activation (26,27). The results of the present study revealed that CORM-3 partially reversed the increase in mtDNA levels and the decreased mitochondrial integrity after HSR compared with iCORM-3. NLRP3-ASC and pro-caspase-1-ASC interactions were also inhibited by CORM-3, suggesting that the mechanism of CORM-3 against neuronal pyroptosis may be associated with an improvement in the dysmorphic mitochondria-induced mtDNA release and an inhibition of the activation of pro-caspase-1/NLRP3/ASC inflammasomes.

Ischemia/reperfusion injury induces the release of neurotoxic amounts of glutamate and causes neuronal calcium overload, mtDNA leakage and mitochondrial membrane collapse (28,29). NAA, a surrogate marker of mitochondrial status, is a general marker of neuronal integrity viability (30) and a reservoir that maintains glutamate concentration at a safe level and prevents it from reaching excitotoxicity (31). Myoinositol (mI), a glial cell marker, reflects the changes of gliosis (32,33). Regarding the changes of Lip in rat brains, MRS-detectable Lip/Cr ratio is elevated after ischemic injury (34). A model of cardiac arrest has revealed that CO markedly increases ATP and phosphocreatine levels following reperfusion, and this mechanism may be associated with the CO-induced improvement of mitochondrial metabolism (35). In addition, exogenous CO administration increased the ATP content and improved oxidative phosphorylation and mitochondrial dysfunction in an ischemia/reperfusion astrocyte model (36). In the present study, increased mI/Cr and Lip/Cr ratios, as well as ATP content and a decreased NAA/Cr ratio were observed in the hippocampus of HSR-treated rats. CORM-3 significantly partially reversed these changes. Therefore, the protective effect of CORM-3 against neuronal pyroptosis may be associated with metabolic reservation after HSR.

There were several limitations to the present study. First, only one model of incomplete ischemia/reperfusion injury inducing neuronal pyroptosis in the hippocampus was included. Other models of incomplete ischemia/reperfusion, such as bilateral common carotid artery occlusion (37), should be further studied. Additionally, the present data only revealed that pro-caspase-1/NLRP3/ASC inflammasomes may be associated with the neuroprotective effects of CORM-3 against pyroptosis; the role of NLRP3 activated by mitochondrial dysfunction should be further studied using NLRP3-knockout mice. In addition, the present study did not focus on whether pyroptosis depended on GSDMD and caspase-11 signaling pathways (38). Further studies on other models and feasible signaling pathways should be performed.

In conclusion, the results of the present study demonstrated that treatment with CORM-3 ameliorated the impairments of locomotor and exploratory activities in a rat model of HSR. This mechanism may be associated with the inhibition of mitochondrial DNA-induced pyroptosis via improvements in cell metabolism.

Acknowledgements

Not applicable.

Funding

The present study is supported by National Natural Science Foundation of China (81701296).

Availability of data and materials

All data generated and analyzed during the present study are included in this published article.

Authors' contributions

LF, LMZ, LQK and FHL designed the study. LQK, LF, LMZ, YL and YCS edited the manuscript. DXZ and LMZ performed statistical analysis. LF, DXZ, LMZ, YL, XPW, WCZ, CXG, XDW and XJK performed the experiments and data collection. All authors read and approved the final manuscript.

Ethics approval and consent to participate

The National Institutes of Health Guidelines for the Care and Use of Laboratory Animals were followed while performing all animal experiments in this study. The Animal Review Board of Cangzhou Central Hospital provided formal approval to conduct the experiments.

Patient consent for publication

Not applicable.

Competing interests

The authors declare that they have no competing interests.

References

1. Demuro JP, Simmons S, Jax J and Gianelli SM: Application of the shock index to the prediction of need for hemostasis intervention. Am J Emerg Med 31: 1260-1263, 2013.
2. Singhal AK, Abrams JD, Mohara J, Hasz RD, Nathan HM, Fisher CA, Furukawa S and Goldman BI: Potential suitability for transplantation of hearts from human non-heart-beating donors: Data review from the gift of life donor program. J Heart Lung Transplant 24: 1657-1664, 2005.

3. Dexter F, Hindman BJ, Cutkomp J and Smith T: Blood warms as it flows retrograde from a femoral cannulation site to the carotid artery during cardiopulmonary bypass. Perfusion 9: 393-397, 1994.
4. Yoshioka M, Itoh Y, Mori K, Ueno K, Matsumoto M and Togashi H: Effects of an interleukin-1beta analogue [Lys-D-Pro-Thr], on incomplete cerebral ischemia-induced inhibition of long-term potentiation in rat hippocampal neurons in vivo. Neurosci Lett 261: 171-174, 1999.
5. Bergsbaken T1, Fink SL, den Hartigh AB, Loomis WP and Cookson BT: Coordinated host responses during pyroptosis: caspase-1-dependent lysosome exocytosis and inflammatory cytokine maturation. J Immunol 187: 2748-2754, 2011.
6. Sekerdag E, Solaroglu I and Gursoyozdemir Y: Cell death mechanisms in stroke and novel molecular and cellular treatment options. Curr Neuropharmacol 16: 1396-1415, 2018.
7. Yang JR, Yao FH, Zhang JG, Ji ZY, Li KL, Zhan J, Tong YN, Lin LR and He YN: Ischemia-reperfusion induces renal tubule pyroptosis via the CHOP-caspase-11 pathway. Am J Physiol Renal Physiol 306: F75-F84, 2014.
8. Xia P, Pan Y, Zhang F, Wang N, Wang E, Guo Q and Ye Z: Pioglitazone confers neuroprotection against ischemia-induced pyroptosis due to its inhibitory effects on HMGB-1/RAGE and Rac1/ROS pathway by activating PPAR-γ. Cell Physiol Biochem 45: 2351-2368, 2018.
9. Schallner N, Fuchs M, Schwer CI, Loop T, Buerkle H, Lagrèze WA, van Oterendorp C, Biermann J and Goebel U: Postconditioning with inhaled carbon monoxide counteracts apoptosis and neuroinflammation in the ischemic rat retina. PLoS One 7: e46479, 2012.
10. R Oliveira S, Queiroga CS and Vieira HL: Mitochondria and carbon monoxide: Cytoprotection and control of cell metabolism-a role for Ca(2+) ? J Physiol 594: 4131-4138, 2016.
11. Choi EY, Choe SH, Hyeon JY, Choi JI, Choi IS and Kim SJ: Carbon monoxide-releasing molecule-3 suppresses *Prevotella intermedia* lipopolysaccharide-induced production of nitric oxide and interleukin-1β in murine macrophages. Eur J Pharmacol 764: 22-29, 2015.
12. Lee DW, Shin HY, Jeong JH, Han J, Ryu S, Nakahira K and Moon JS: Carbon monoxide regulates glycolysis-dependent NLRP3 inflammasome activation in macrophages. Biochem Biophys Res Commun 493: 957-963, 2017.
13. Zhang W, Tao A, Lan T, Cepinskas G, Kao R, Martin CM and Rui T: Carbon monoxide releasing molecule-3 improves myocardial function in mice with sepsis by inhibiting NLRP3 inflammasome activation in cardiac fibroblasts. Basic Res Cardiol 112: 16, 2017.
14. Latz E, Xiao TS and Stutz A: Activation and regulation of the inflammasomes. Nat Rev Immunol 13: 397-411, 2013.
15. Zhang LM, Zhang DX, Fu L, Li Y, Wang XP, Qi MM, Li CC, Song PP, Wang XD and Kong XJ: Carbon monoxide-releasing molecule-3 protects against cortical pyroptosis induced by hemorrhagic shock and resuscitation via mitochondrial regulation. Free Radic Biol Med 141: 299-309, 2019.
16. Zhang LM and Zhang DX: The dual neuroprotective-neurotoxic effects of sevoflurane after hemorrhagic shock injury. J Surg Res 235: 591-599, 2019.
17. Ampawong S, Isarangkul D and Aramwit P: Sericin ameliorated dysmorphic mitochondria in high-cholesterol diet/streptozotocin rat by antioxidative property. Exp Biol Med (Maywood) 242: 411-421, 2017.
18. Mariappan N, Soorappan RN, Haque M, Sriramula S and Francis J: TNF-α-induced mitochondrial oxidative stress and cardiac dysfunction: Restoration by superoxide dismutase mimetic Tempol. Am J Physiol Heart Circ Physiol 293: H2726-H2737, 2007.
19. Hao P, Liang Z, Piao H, Ji X, Wang Y, Liu Y, Liu R and Liu J: Conditioned medium of human adipose-derived mesenchymal stem cells mediates protection in neurons following glutamate excitotoxicity by regulating energy metabolism and GAP-43 expression. Metab Brain Dis 29: 193-205, 2014.
20. Zhang DX, Zhang LM, Zhao XC and Sun W: Neuroprotective effects of erythropoietin against sevoflurane-induced neuronal apoptosis in primary rat cortical neurons involving the EPOR-Erk1/2-Nrf2/Bach1 signal pathway. Biomed Pharmacother 87: 332-341, 2017.
21. Kawanishi S, Takahashi T, Morimatsu H, Shimizu H, Omori E, Sato K, Matsumi M, Maeda S, Nakao A and Morita K: Inhalation of carbon monoxide following resuscitation ameliorates hemorrhagic shock-induced lung injury. Mol Med Rep 7: 3-10, 2013.
22. Chamorro V, Pandolfi R, Moreno L, Barreira B, Martínez-Ramas A, Morales-Cano D, Ruiz-Cabello J, Lorente JA, Duarte J, Cogolludo Á, *et al*: Effects of quercetin in a rat model of hemorrhagic traumatic shock and reperfusion. Molecules 21: pii: E1739, 2016.
23. Hu X, Wang J, Zhang Q, Duan X, Chen Z and Zhang Y: Postconditioning with sevoflurane ameliorates spatial learning and memory deficit after hemorrhage shock and resuscitation in rats. J Surg Res 206: 307-315, 2016.
24. Zheng G, Zhan Y, Wang H, Luo Z, Zheng F, Zhou Y, Wu Y, Wang S, Wu Y, Xiang G, *et al*: Carbon monoxide releasing molecule-3 alleviates neuron death after spinal cord injury via inflammasome regulation. EBioMedicine 40: 643-654, 2019.
25. Jabaut J, Ather JL, Taracanova A, Poynter ME and Ckless K: Mitochondria-targeted drugs enhance Nlrp3 inflammasome-dependent IL-1β secretion in association with alterations in cellular redox and energy status. Free Radic Biol Med 60: 233-245, 2013.
26. Xi H, Zhang Y, Xu Y, Yang WY, Jiang X, Sha X, Cheng X, Wang J, Qin X, Yu J, *et al*: Caspase-1 inflammasome activation mediates homocysteine-induced pyrop-apoptosis in endothelial cells. Circ Res 118: 1525-1539, 2016.
27. Ahn H, Kim J, Kang SG, Yoon SI, Ko HJ, Kim PH, Hong EJ, An BS, Lee E and Lee GS: Mercury and arsenic attenuate canonical and non-canonical NLRP3 inflammasome activation. Sci Rep 8: 13659, 2018.
28. Kravcukova P, Danielisova V, Nemethova M, Burda J and Gottlieb M: Transient forebrain ischemia impact on lymphocyte DNA damage, glutamic acid level, and SOD activity in blood. Cell Mol Neurobiol 29: 887-894, 2009.
29. Lehotský J, Racay P, Pavlíková M, Tatarková Z, Urban P, Chomová M, Kovalská M and Kaplán P: Cross-talk of intracellular calcium stores in the response to neuronal ischemia and ischemic tolerance. Gen Physiol Biophys 28: F104-F114, 2009.
30. Signoretti S, Marmarou A, Tavazzi B, Lazzarino G, Beaumont A and Vagnozzi R: N-Acetylaspartate reduction as a measure of injury severity and mitochondrial dysfunction following diffuse traumatic brain injury. J Neurotrauma 18: 977-991, 2001.
31. Ory-Lavollée L, Blakely RD and Coyle JT: Neurochemical and immunocytochemical studies on the distribution of N-acetyl-aspartylglutamate and N-acetyl-aspartate in rat spinal cord and some peripheral nervous tissues. J Neurochem 48: 895-899, 1987.
32. Chang C and Jang T: Age-dependent neurotoxicity of striatal lesions produced by aminooxyacetic acid: Quantitative in vitro 1H NMR spectroscopic studies. J Neurochem 65: 1192-1198, 1995.
33. Mierisová S and Ala-Korpela M: MR spectroscopy quantitation: A review of frequency domain methods. NMR Biomed 14: 247-259, 2001.
34. Harada K, Honmou O, Liu H, Bando M, Houkin K and Kocsis JD: Magnetic resonance lactate and lipid signals in rat brain after middle cerebral artery occlusion model. Brain Res 1134: 206-213, 2007.
35. Lavitrano M, Smolenski RT, Musumeci A, Maccherini M, Slominska E, Di Florio E, Bracco A, Mancini A, Stassi G, Patti M, *et al*: Carbon monoxide improves cardiac energetics and safeguards the heart during reperfusion after cardiopulmonary bypass in pigs. FASEB J 18: 1093-1095, 2004.
36. Almeida AS, Queiroga CS, Sousa MF, Alves PM and Vieira HL: Carbon monoxide modulates apoptosis by reinforcing oxidative metabolism in astrocytes: Role of Bcl-2. J Biol Chem 287: 10761-10770, 2012.
37. Chai H, Schultz G, Aghaie K and Zhou W: In vivo assessment of the effects of ginsenoside Rb1 on intimal hyperplasia in ApoE knockout mice. J Surg Res 162: 26-32, 2010.
38. Feng S, Fox D and Man SM: Mechanisms of gasdermin family members in inflammasome signaling and cell death. J Mol Biol 430: 3068-3080, 2018.